SLAC-PUB-15998

MOGA Optimization of LCLS2 Linac

Lanfa Wang, Paul Emma and Tor O. Raubenheimer

SLAC National Accelerator Laboratory

June 2014

Presented at the FEL 2014
Basel, Switzerland, 25-29 August 2014

Work supported in part by US Department of Energy under contract DE-AC02-76SF00515.

MOGA Optimization of LCLS2 Linac

Lanfa Wang, Paul Emma and Tor O. Raubenheimer

SLAC National Accelerator Laboratory

This paper briefly summarizes the preliminary optimization study on the configurations of LCLSII with superconducting cavity. The setup of each configuration is first optimized using Multi-Objective Genetic Algorithm (MOGA) and Litrack code, which includes the longitudinal phase space only. For each operation mode, MOGA is applied to optimize the machine parameters in order to to get flat top current profile and zero energy chirp at the beginning of the undulator. The geometric wake of the RF cavities and resistive wall wake of the beam pipe are included, but the CSR wake is not there yet. Finally, ELEGANT code is used to do full 3-dimension particle simulation, which includes the CSR and ISR effect. Therefore, the emittance growth due to CSR can be checked.

I. Nonlinear Beam from Injector

In the current design, the injector of LCLS2 uses CW normal conducting RF gun. The strong space charge effect at the injector induces large nonlinearity in the longitudinal phase space. The dominant one is cubic term, which is the fundamental term of the longitudinal space charge effect. The high order terms also have large contributions to the linac beam dynamics. These nonlinear effects are amplified throughout the linac when the bunch is compressed. The strong space charge effect makes LCLS2 beam largely different from the existing LCLS beam and more difficult in the design. As results, the design of linac beam has strong dependence on the injector beam.

The longitudinal phase space, current profile and B_{mag} along the bunch at linac with 98MeV beam are shown in Fig. 1. For three bunch charges: 20pC, 100pC and 300pC. The overall bunch profile is similar: there is a long bunch tail. The nonlinearity can be clearly seen after extracting the linear chirp and RF curvature as shown in Fig.2. Table 1 summarizes the high order terms for different bunch charges and peak currents. The nonlinearity, except the last case, is about proportional to the peak current. The 20pC bunch charge with 10A peak current has larger nonlinearity, which makes it difficult to provide good quality beam for FEL. For this reason, a lower peak current of 4.5A is chosen for 20pC to reduce the space charge effect.

The strong space charge also causes mismatching along the bunch, especially for 20pC case where the space charge is stronger. However, the core bunch still has good matching. When the beam passes through the linac, the collective effects add more mismatching to the beam. We shall estimate the mismatching effect of the injector beam on the FEL performance later.

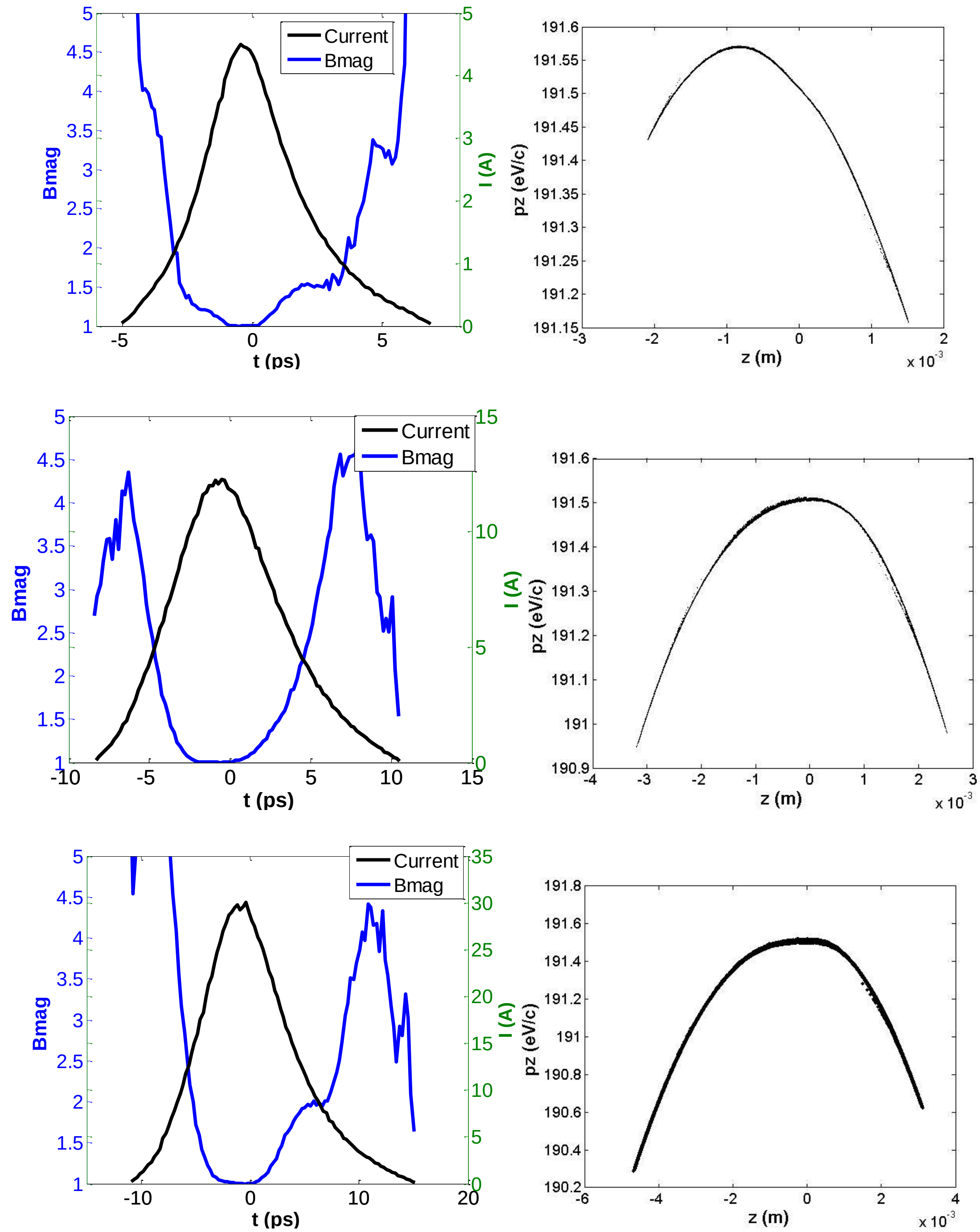

Fig. 1: Phase space and current profile at the exit of injector linac (98MeV) after the injector for 20pC (top), 100pC (middle) and 300pC (bottom) bunch charge. Bunch head is to the left.

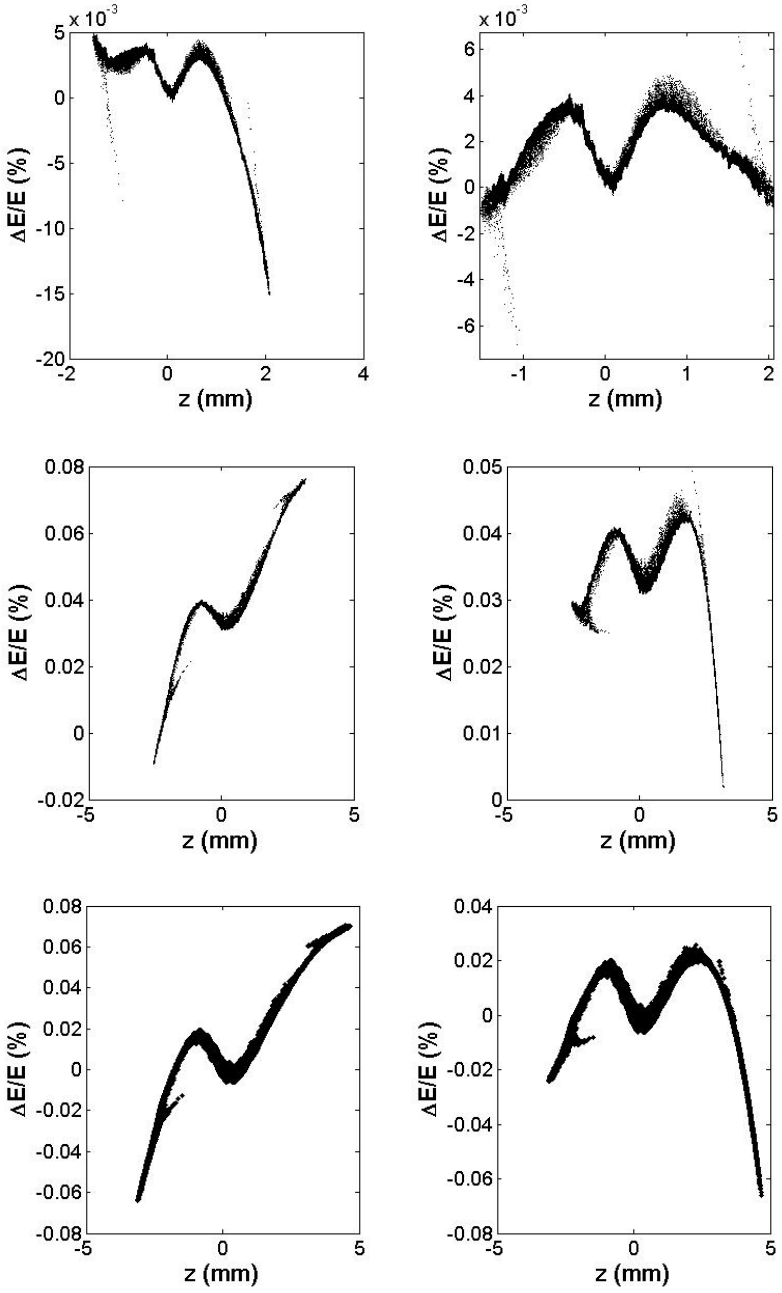

Fig. 2: 3rd-order term (left column) and high order terms (right column) at the exit of injector linac (98MeV) after the injector for 20pC (top), 100pC (middle) and 300pC (bottom) bunch charge.

Table 1: cubic and high order terms for different beam from injector (at 98MeV)

Bunch charge/peak current	**$\delta(\Delta E/E)$ 3rd order**	**$\delta(\Delta E/E)$ high orders**	**ΔE high orders**
20pC (I_{pk}4.5A)	2×10^{-5}	1×10^{-5}	3.9keV
100pC (I_{pk} 12A)	9×10^{-5}	4×10^{-5}	9keV
300pC (I_{pk} 31A)	1.5×10^{-4}	9×10^{-5}	29keV
20pC (I_{pk}10A)	1.2×10^{-4}	8×10^{-5}	39keV

II. Resistive Wall Wake fields as a strong de-chirper

The wake fields play an important role in the beam dynamics: increases the nonlinearity and de-chirper the beam. Fig. 1 shows the longitudinal wake in the 1.3GHz SC cavity and the 3.9GHz SC cavity, which is used to linearize the phase space before BC1. The linearizer has much stronger wake. The wake fields used in both Litrack and Elegant are shown to make sure that they are the same. They are almost identical except the range of the wake.

The resistive wall (RW) wake plays an important role to de-chirper the beam. Table 2 lists the contributions of the resistive wall wake, which is dominant by the 2km-long bypass line. The beam is chirped along Linac 1 and Linac 2 by RF cavities in order to compress the beam. This positive chirped beam is naturally de-chirped by the resistive wall wake after Linac 3 if the design is optimal. This is a nice feature of LCLSII design. However, this also put a strong limit on the design since the wake field cannot be adjusted. The large de-chirp effect due to the resistive wall wake requires enough chirper to be provided by the RF cavities. For 1kA peak current of flat beam, the energy loss due to the resistive wall wake are 4.8MV, 18MV, 34MV for 20pC, 100pC and 300pC, respectively.

The strong de-chirp of RW wake sets a tight constraint in the linac design. Since the wake field is not adjustable and it seems it is too strong in most case. There is no need for additional de-chirper. Instead, it requires the linac RF to provide large enough energy chirp to compensate the RW effect, which adds a constraint in the set-up of the bunch compressor systems. Indeed, the design of the BCs are strongly depends on the RW wake.

Besides the energy loss due to the resistive wall wake, the RW wake can spoil the phase space. The nonlinear wake filed for a longer bunch (>100μm) causes strong distortion in phase space. This makes it difficult to provide high quality long bunch, for instance, 300pC bunch charge with peak current 500A. The RW wake with aluminum pipe has stronger nonlinearity and it would be

good to replace it with stainless steel material or surface coating. Furthermore, when the beam has strong double horn in current profile, the RW wake also induces strong nonlinear de-chirper.

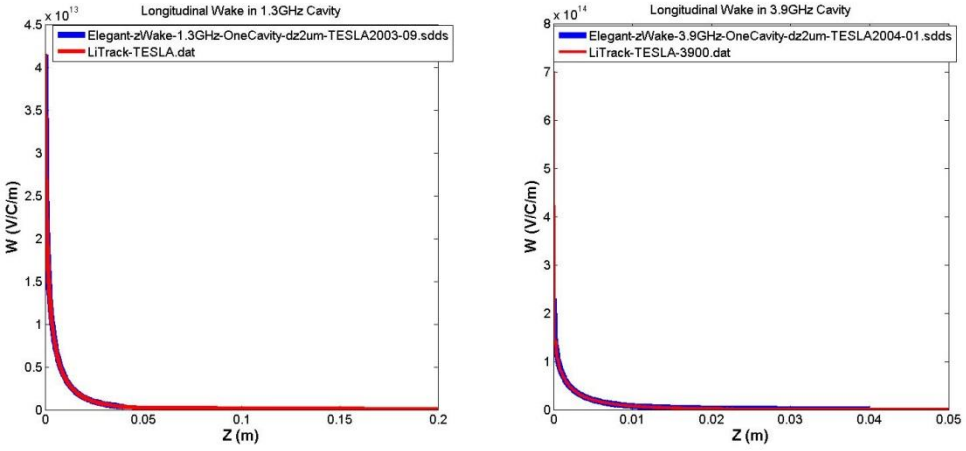

Fig. 1. Longitudinal wake field in the 1.3GHz and 3.9GHz cavities.

Table 2: Resistive wake along the linac

Beam line Section	Pipe Length (m)	Pipe Radius (mm)	Material	Conductivity (Ohm-m)	Time Constant (fs)	Peak Energy Loss (MeV)
Linac Extension	353	24.5	stainless	1.37×10^{6}	5	1.2
Rolled Dog-Leg #1	50	12.7	stainless	1.37×10^{6}	5	0.5
Bypass Line	2193	24.5	stainless	1.37×10^{6}	5	12.06
DL & LTU to SXRSS Und.	382	12.7	aluminum	3.60×10^{7}	5	4

III. MOGA optimization

The fast speed of Litrack code is used in the MOGA optimization [1]. The CSR is not included. Table 3 summarizes the main parameters of the optimized configurations. The strategy of the optimization aims to reduce the RF power while providing a similar beam quality: flat current profile and smaller energy spread (zero energy chirper). A new baseline, which tends to reduce the R56 at BC2 by increasing the compression factor at BC1 in order to mitigate the CSR at BC2, is also added to show the range of the parameters. It uses different RW wakes.

The energy losses due to CSR at BC1 and BC2 are also listed in the table (detail see next section). The power is calculated for two cases: the repetition rates in the initial phase are 929 kHz, 625 kHz and 210 kHz for 20pC, 100pC and 300pC, respectively; the final repetition rates are 929 kHz for all bunch charges. The energy loss in BC1 is about 1W for 100pC and 3W for

300pC. The maximum power loss in BC2 is about 117 W for 300pC charge, which can become even larger when larger peak currents are applied in the future.

Fig. 2 shows the phase space and current profile the beginning of the undulator by Litrack. The current profiles are all flat except 20pC case. These flat current profiles are essential for the self-seeding. There are also always near zero energy chipper for the core part of bunches.

Table 3: Configurations for BC1 energy 250MeV and BC2 energy 1.6GeV, without de-chirper

	20pC, 500A	100pC, 1kA	100pC, 1kA,New baseline	100pC,1.5kA	300pC, 1kA	300pC, 600A
$\phi_{L1}(^\circ)$	-21	-21	-12.2	-21.9	-19.85	-20
$\phi_{Linearizer}(^\circ)$	-165	-165	-150	-164.5	-162.2	-162
$\phi_{L2}(^\circ)$	-21.1	-21	-21.1	-28.4	-28.86	-29
$\phi_{L3}(^\circ)$	0	0	0	0	0	0
V_{L1} (MV)	219.6	219.6	216	225	222	222
$V_{Linearizer}$ (MV)	54.78	54.78	64.90	58.7	59.58	59.58
V_{L2} (GV)	1.447	1.447	1.447	1.5349	1.5418	1.5418
V_{L3} (GV)	2.4	2.4	2.4	2.4	2.4	2.4
BC1 R_{56} (mm)	-53	-55	-55	-53.46	-47.4	-44.7
BC2 R_{56} (mm)	-61.8	-60	-37.5	-45.5	-49.2	-49.2
σ_{z0} (mm)	0.627	1.02	1	1.02	1.30	1.30
I_{pk0} (A)	4.5	12	12	12	31	31
σ_z^{BC1}(mm)	0.187	0.283	0.15	0.246	0.43	0.48
I_{pk}^{BC1} (A)	15	43	82	50	91	82
σ_E^{BC1}(%)	0.835	1.36	1.6	1.469	1.857	1.857
σ_z^{BC2}(μm)	5.16	8.85	9.2	5.516	29	48
I_{pk}^{BC2} (kA)	0.515	1.355	1.36	2.723	1.18	0.75
σ_E^{BC2}(%)	0.295	0.458	0.378	0.53	0.822	0.884
σ_E^{UndBEG}(%)	0.055	0.065	0.066	0.079	0.239	0.346
$P_E^{BC1CSR}\ (phase1)(W)$		0.62		0.63	0.63	0.63
$P_E^{BC1CSR}\ (phase2)(W)$		0.92		0.93	2.79	2.79
$P_E^{BC2CSR}\ (phase1)(W)$		28		58	27	19
$P_E^{BC2CSR}\ (phase2)(W)$		42		88	117	84

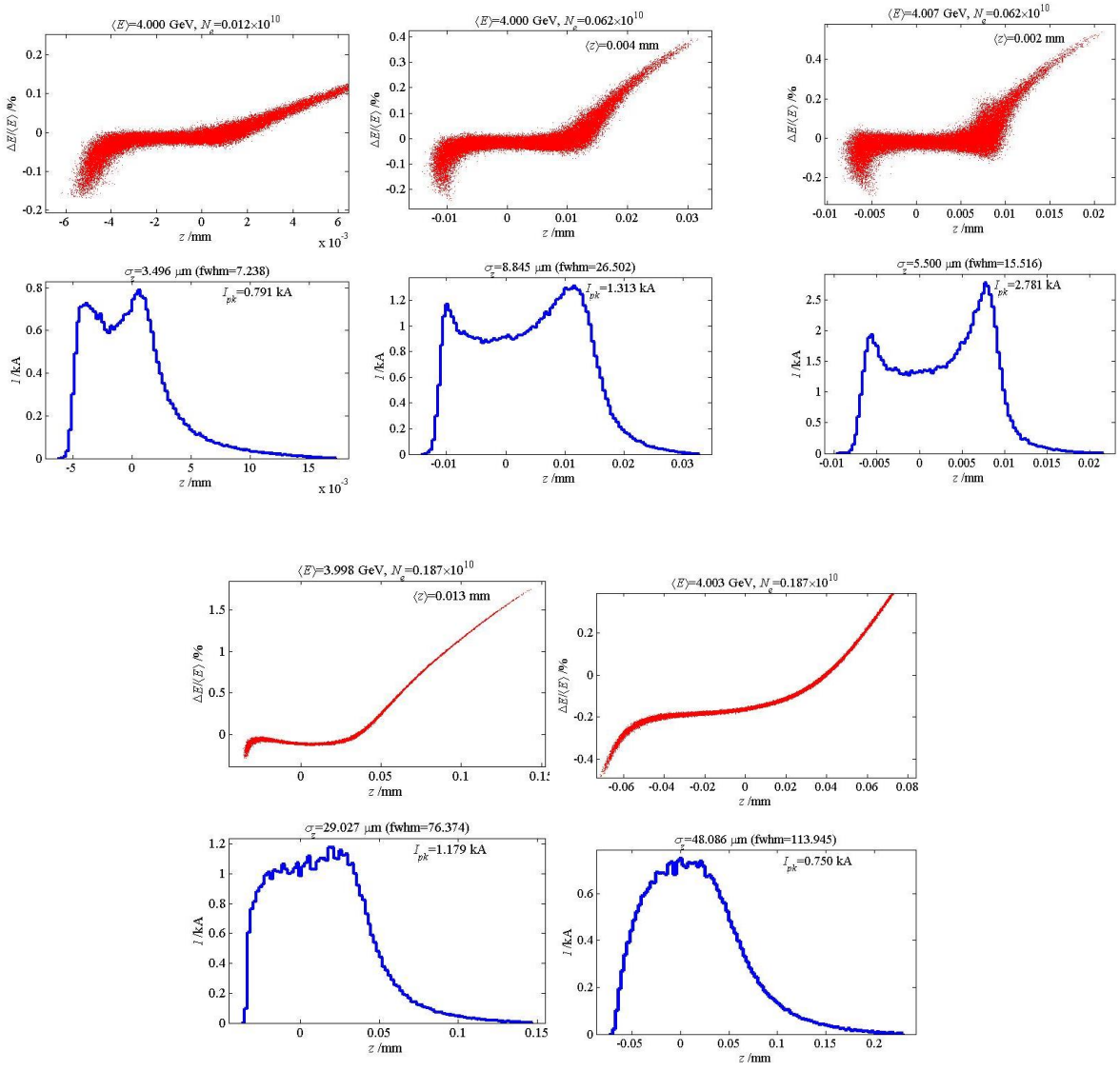

Fig. 2. Phase space before the undulator for different configurations (from top to bottom: 20pC@500A, 100pC@1kA, 100pC@1.5kA, 300pC@1kA, 300pC@700A)

IV. Final Beam with CSR

After getting satisfied solutions from MOGA optimization, we use ELEGANT to track particles 3-dimensionaly. Besides wake fields, the CSR and ISR are included. The CSR changes the beam current profile and some parameters are tweaked to get flat top current profile.

BC1 and BC2 are located along the Superconducting Linac. Therefore, the energy loss there due to CSR need to be evaluated. The energy loss due to CSR at the 2nd bunch compressor (BC2) is large due to the high peak current there. The radiation can propagate to the downstream and

heat the SFR cryomodule. The ISR in general is much smaller compared with the CSR. Unlike a true wake, each particle is affected only by those behind it. Also unlike true wakes, the effects of CSR depend on the slope of the bunch distribution λ'. The steady status CSR is relatively simple and can be written as

$$W(s) = -\frac{2e^2}{(3R^2)^{1/3}} \int_{-\infty}^{\infty} \frac{d\lambda}{dz} \frac{dz}{(s-z)^{1/3}} \tag{1}$$

The reality of CSR in a bunch compressor is much more complicted than the 1-D steady state result. The transient effects entering bend magnets and the propagation of CSR through drifts following the bending magnets and the variation of bunch profile are all important. Furthermore, the CSR affects the transverse dynamics throughout the bunch compressor where the transverse beam size and beam optics vary. The simple steady status model can greatly underestimate the CSR effect in some case. The estimation of CSR in the paper includes all aboves factors by tracking the particles through the bunch compressors.

The total energy loss at BC2 for various configurations is listed in Table. 3. Fig. 3 shows the detail of the energy loss along the bunch (bunch head is on the left) for different configurations. Note that it is total energy change throughout BC2, including the transient effect. The current profile is at end of the BC2. The energy loss is highly correlated with the current profile as expected. For instance, the double horn in the current profile induces similar shape in the energy loss distribution.

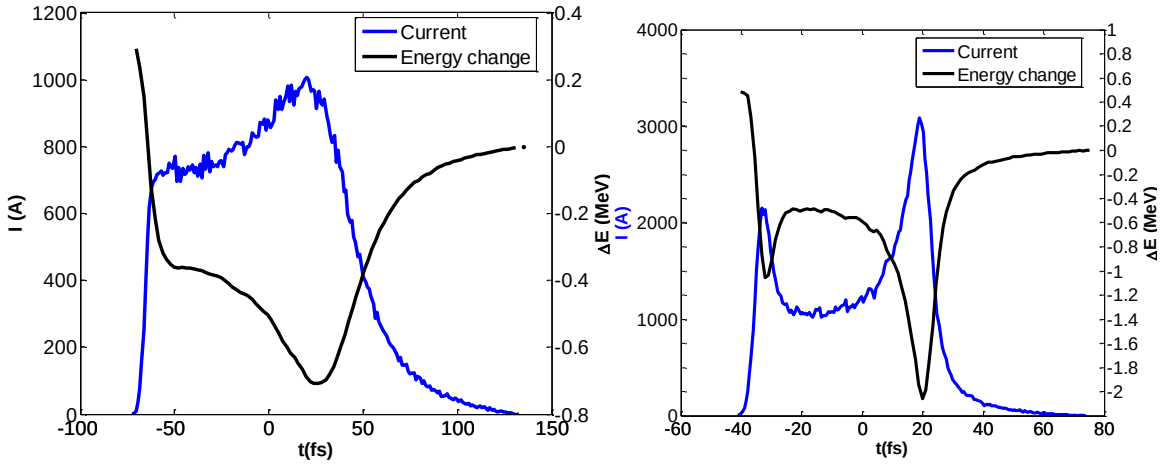

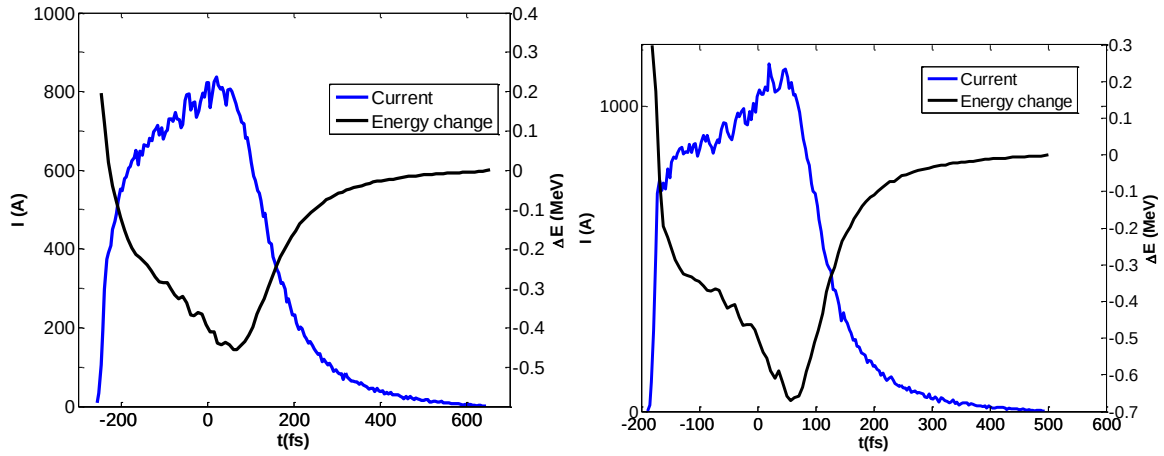

Fig. 3. Energy change due to CSR at whole BC2 for 100pC, 1kA(top left); 100pC, 1.5kA(top right); 300pC,700A(bottom left); 300pC,1kA(bottom right). The bunch shape is also shown, with the head to the left (the blue curve).

The longitudinal motion is coupled to the transverse plane via nonzero dispersion functions η, η′ and the energy change due to CSR induced in the bending magnets. At the end of the bunch compressor, the transverse displacement and the angle deviation of bunch slice at position *s* will be

$$\Delta x(s) = \frac{1}{E_0}\int \eta \frac{dE_{CSR}(s)}{dz} dz, \tag{2}$$

$$\Delta x'(s) = \frac{1}{E_0}\int \eta' \frac{dE_{CSR}(s)}{dz} dz\ . \tag{3}$$

Different from traditional magnet kicker, the CSR induced kicker varies along the bunch and this non-uniform CSR kicker along the bunch causes a growth of the projected emittance. Fig. 4-8 show the longitudinal phase space, beam profile and sliced emittance of the beam at the beginning of the undulator for various configurations. The simulations are done with ELEGANT code which includes the geometric wake fields, resistive wakes, ISR and CSR.

In 20pC case (FIG.4), the distortion of the phase space is due to the resistive wall (RW) wake. The RW wake de-chirp the beam, however, this de-chirper strongly depends on the beam profile and has large nonlinearity when the current profile is far from flat shape. There is no emittance growth due to CSR for this beam.

The configuration of 100pC@1kA listed (FIG.5) has very small emittance growth due to CSR. The peak current is slightly lower than the Litrack version in order to reduce emittance growth.

The configuration of 300pC bunch charge with 700A (FIG.8) is very good, which has zero emittance growth. FEL simulation confirms that this configuration is good. For 1kA peak current (FIG.7), the sliced emittance at the head of bunch is slight spoiled. However, the emittance in most part of bunch is very good.

For high peak current, such as 100pC 1.5KA configuration (FIG.6), the emittance growth is large, which need to be reduced by optimizing the configuration or using asymmetric 5-bends BC2. There are a number ways to minimize the emittance growth due to CSR: cancellation CSR induced transverse kickers by adjusting the phase advance of two CSR sections [2, 3], compensation of CSR kickers using compressors which offer opposite signs of the dispersions [4, 5], minimization of the H-function ($H = \eta^2 + (\beta\eta' + \alpha\eta)^2/\beta$) of the bunch compressor [6]. The first approach works when the CSR of two sections are on the same level. The CSR after DL2 can be used to partially compensate the CSR effect at BC2. The second approach belongs to local compensation and requires an optimal design of the beam optics. Jing's approach uses zigzag-type compressor and the optimized emittance growth is 27% [4]. Khan's method use 5-bending magnets asymmetrical BC and it can completely suppress the emittance growth. The traditional 4-magnets asymmetric BC doesn't work well on reduction of the emittance growth due to CSR due to the limitation of the same sign of dispersion function. The third approach (minimization of the H-function) can be used as a general guide for the optimal design of the beam optics in BCs. We haven't applied any the above methods in the current beam optics design. We are applying these schemes in the new optics design.

Fig. 9 shows an example of the emittace minimization using Khan's 5-bends asymmetric BC2 scheme for 100pC bunch charge with 1.5kA peak current. The emittance growth (shown in Fig. 6) with traditional BC2 is completely suppressed with Khan's symmetric BC.

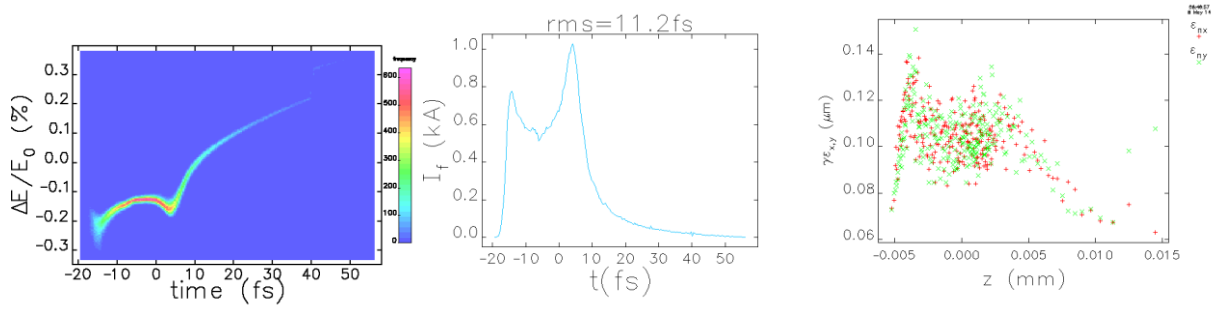

Fig. 4 Phase space before undulator from Elegant simulation for 20pC beam with 600A peak current

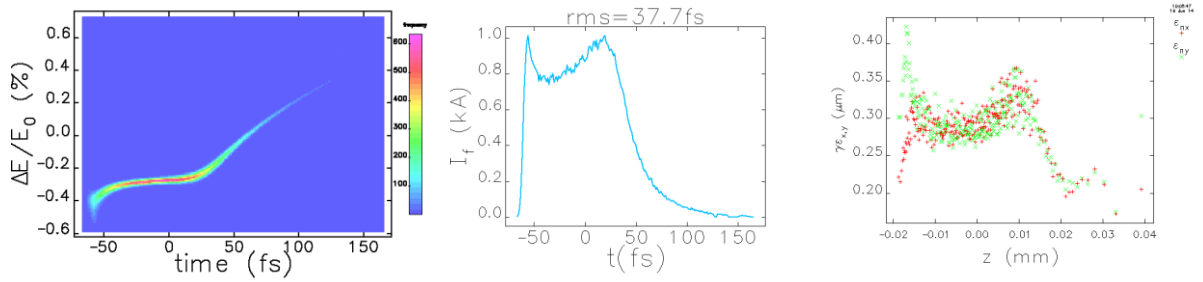

Fig. 5 Phase space before undulator from Elegant simulation for 100pC beam with 1.0kA peak current, R56 at BC2 is adjusted to -58.8mm to reduce the CSR effect, L2 phase -30 degree

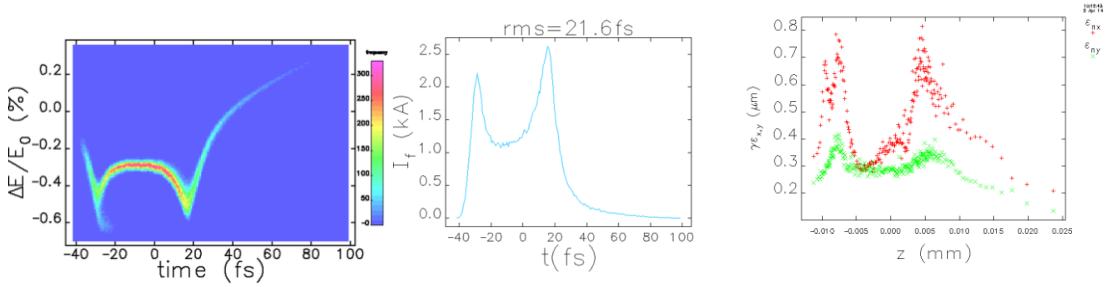

Fig. 6 Phase space before undulator from Elegant simulation for 100pC beam with 1.5kA peak current

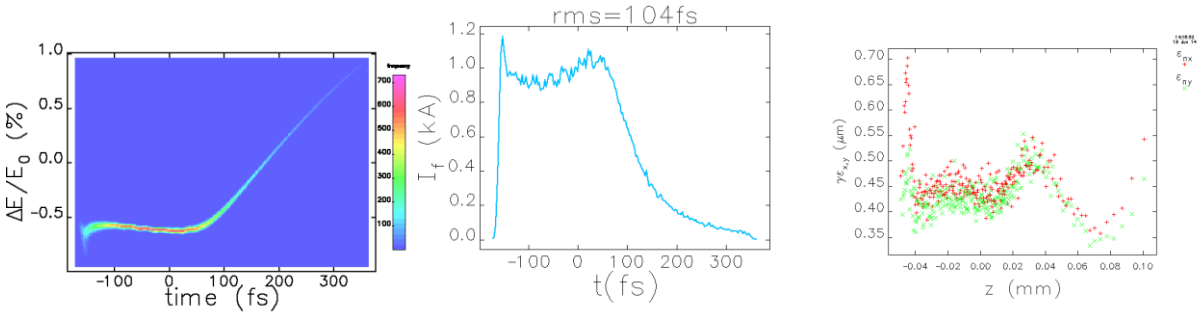

Fig. 7 Phase space before undulator from Elegant simulation for 300pC beam with 1kA peak current

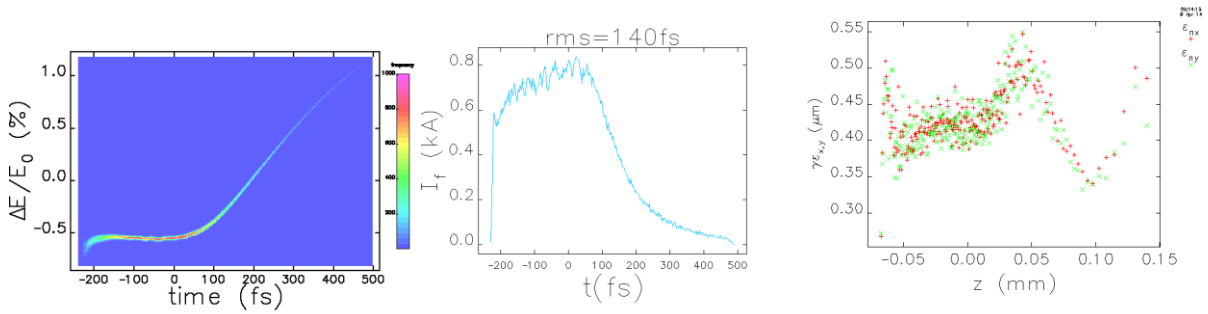

Fig. 8 Phase space before undulator from Elegant simulation for 300pC beam with 700A peak current

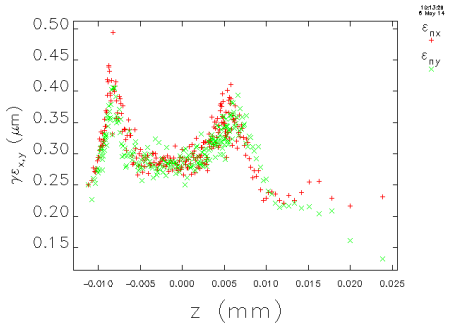

Fig. 9: Slice emittance at the beginning of undulator with asymmetric bunch compressor for 100pC 1.5kA case.

V. Towards high peak current

Preliminary study shows that it is bit of challenge to set-up high peak current configuration. Besides the projected emittance growth due to CSR, the large energy loss can distort the phase space, for instance 100pC with 1.5kA case shown in Fig. 5. There is no simple mitigation for the later. For instance, the peak current at 20pC can be easily above 3kA. Figure 10 shows an example of the ELEGANT simulation. However, the collective effect largely distorts the phase space. This makes the high peak current configuration difficult.

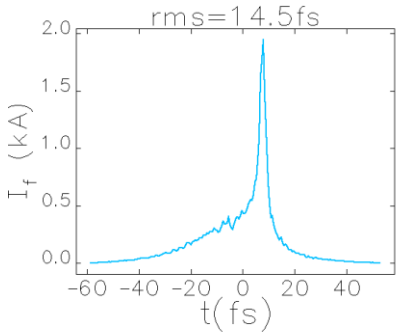

Fig. 10: Current profile of 20pC bunch before the Undulator. Elegant simulation.

VI. Summary and outlook

MOGA is applied to optimize the LCLSII, in order to get flat top current profile and zero energy chirp. Small energy spread, zero energy chirp and flat current profile are achieved for different bunch charges. MOGA provides a very useful tool in the design.

kA flat beams with good emittance are obtained for both 100 pC and 300 pC bunch charge. 20pC bunch has very small emittance, however the peak current with a flat current profile is low.

A single spike with high peak current (>2kA) is possible. In general, the beam quality with low charge is largely spoiled by the collective effects.

In short summary, the emittance growth due to CSR is well controlled for 1kA beams; The resistive wall provides a strong de-chirper and has large impact on the design of LCLSII linac; high peak current need more optimization, including injector; Existing optimizations have been done for fixed energies at BC1 and BC2, We shall further optimize the energies at BCs.

Acknowledgements

Wang thanks Christos Papadopoulos and Feng Zhou for fruitful discussions and providing injector simulation data, M. Nosochkov and M. Woodley for helpful discussions about LCLSII beam optics, and Donish Khan for providing his result with asymmetric BC. This work is supported by Department of Energy Contract No. DE-AC02-76SF00515

Reference

[1] L. Wang and T. O. Raubenheimer, Proceedings of FEL 2013.

[2] E.Saldin et. Al. Instrum. Methods Phys. Res., Sect. A 398 (1997)

[3] D. Douglas, Thomas Jefferson National Accelerator Facility Report No. JLAB-TN-98-012, 1998.

[4]S. Di Mitri, M. Cornacchia, and S. Spampinati, PRL 110, 014801 (2013)

[5]Yichao Jing, Yue Hao, and Vladimir N. Litvinenko, Phys. Rev. STAccel. Beams 16, 060704 (2013)

[6] Donish Khan, private commutations.

[7]S. DiMitri, M.Cornacchia, Instrum. Methods Phys. Res., Sect. A 735, 60(2014)